JOURNAL OF MATERIALS SCIENCE 7 (1972) 793–806

Strongly coupled growth in faceted-nonfaceted eutectics of the monovariant type

P. R. SAHM
Brown Boveri Research Centre, CH-5401 Baden, Switzerland

M. LORENZ
Sulzer Bros. Metallurgical Laboratory, CH-8401 Winterthur, Switzerland

The monovariant eutectic Co, Cr–$Cr_{7-x}Co_xC_3$ fulfils all the usual criteria for a faceted-nonfaceted system (such as Al–Si or Fe–C, for example) and thus would not be expected to show the very strongly coupled growth which is observed. The eutectic morphology can be described by the $\bar{R}^2v = K$ relationship (v = growth rate, $\bar{R}$ = half of average interfibre distance); however, the constant, $K = K(G)$ appear to be a function of the temperature gradient G ahead of the solid-liquid interface. Quenching this interface helped to establish the growth mechanism involved. It was concluded that the interface grows with a relatively large kinetic under-cooling and slightly non-isothermally in that Co, Cr-dendrite tips crystallise out ahead, leaving open a network of voids (such as in a close-packed array of spheres) which are being filled in by the carbide $Cr_{7-x}Co_xC_3$. The large maximum growth rate anisotropy of the fibrous carbide in the [0001] direction, nevertheless, makes the coupled eutectic growth mode a very stable one.

1. Introduction

Utilising monovariant eutectic reactions, a broad class of alloys has been added to directionally-solidifiable simple-binary two-phase materials [1-3]. The best documented work so far has been one on Cr, Co–$Cr_{7-x}Co_xC_3$ alloys [1]. The resulting eutectic structures of these as well as of related alloys of the type Cr, Me–$Cr_{7-x}Me_xC_3$ (with Me = Co, Fe, Ni) turn out to be unusual in several respects.

The outstanding feature of these alloys is the great insensitivity of their directionality to control parameters such as growth rates, temperature gradients, impurity content, the alloy composition itself, etc. With respect to foundrymen's endeavours to control the morphology and properties of cast alloys, this property is a very desirable one. However, in the light of results with other such faceted-nonfaceted eutectics [4], but pertaining to strictly binary systems, this represents an unexpected trait. The objective of this paper, therefore, is seen in the attempt to discuss certain features of the growth-kinetics of Cr, Me–$Cr_{7-x}Me_xC_3$ alloys to explain their strongly coupled crystallisation.

2. Experimental Procedures

The investigated Co–Cr–C alloy compositions were taken from basically four cuts through the monovariant-eutectic line yielding Cr, Co–$Cr_{7-x}Co_xC_3$ two-phase structures (fig. 1). Most of the work was carried out with these Co–Cr–C alloys. Fe-, Ni-, and Mn-containing alloys were prepared only at "strategic points" to confirm results with the Co-alloys. Table I indicates the impurity levels present in the raw materials utilised. Ingots for the directional

TABLE I Trace impurities (less than 0.001 wt%) found spectroscopically in raw materials: Co, Cr, C.

Impurities	Si	Ni	Ca	Cu	Al	Mg	Cr	Ti
Co	×	×	×	×				
Cr	×		×		×	×		
C			×	×		×	×	×

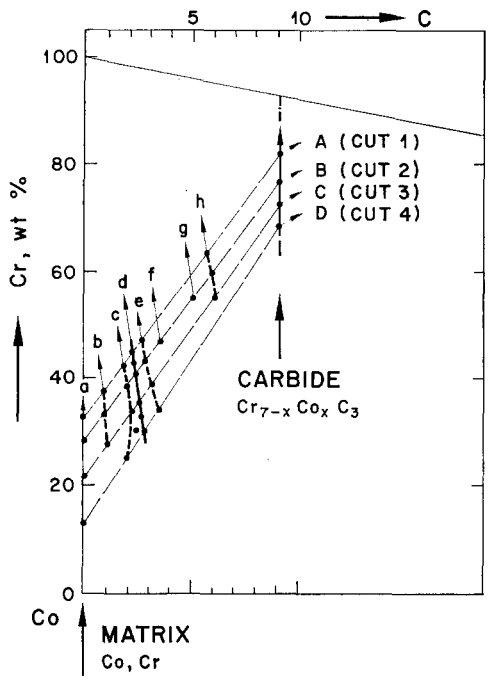

Figure 1 Co–Cr corner of ternary Co–Cr–C system indicating investigated alloys on four cuts through eutectic trough of the Co, Cr (= γ-Co) — $Cr_{7-x}Co_xC_3$ two-phase alloys.

solidification were prepared by sucking melt into quartz tubes, thus quenching them rapidly. The ingots so obtained fitted loosely into the alumina tubes required for the solidification experiments.

The directional solidification was carried out under argon in a simple design using quartz envelopes and alumina tubes (fig. 2). A number of variants of the basic set-up served different purposes. Fig. 2a shows the normal directional solidification apparatus, 2b a modification for quenching in which the sample was held and released for the quench by an electromagnet, 2c a further modification utilising a liquid metal coolant for controlling the temperature gradient at the solid-liquid interface and, lastly, a susceptor heated design for the solidification of very small diameter samples (fig. 2d) with high temperature gradients.

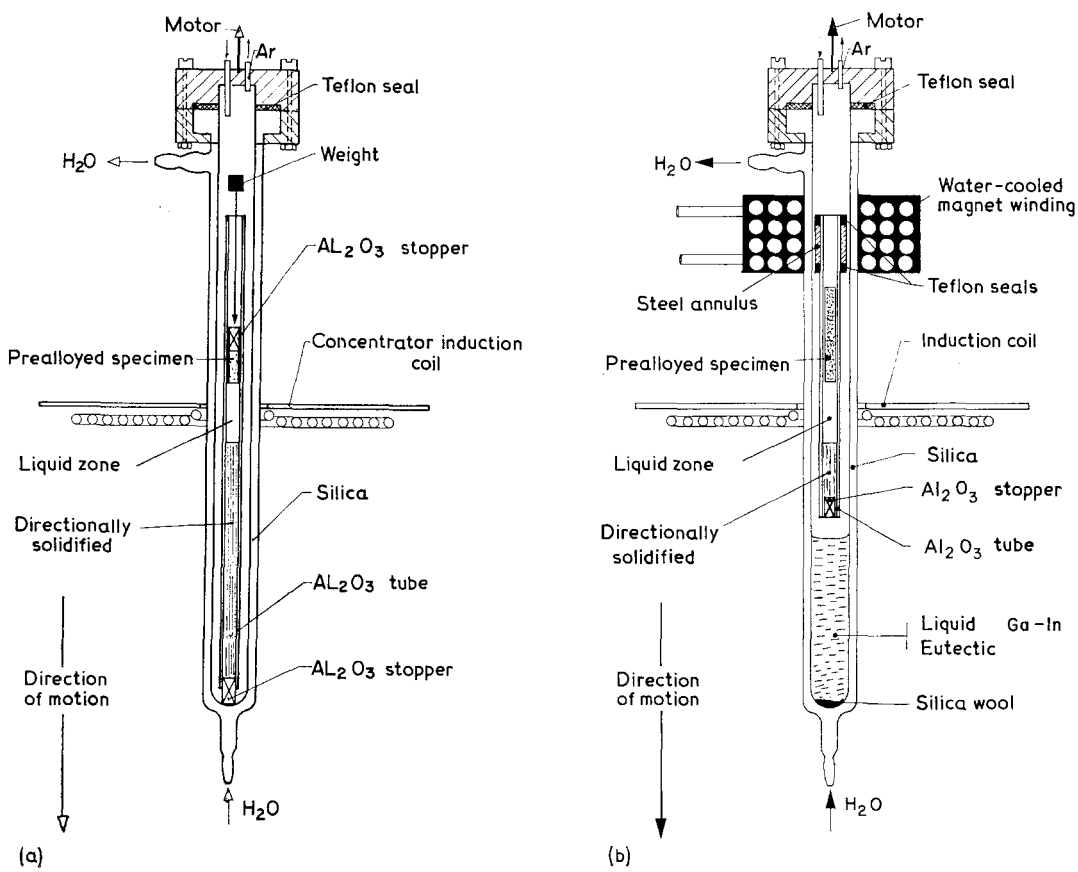

Figure 2 Four experimental set-ups for directional solidification.

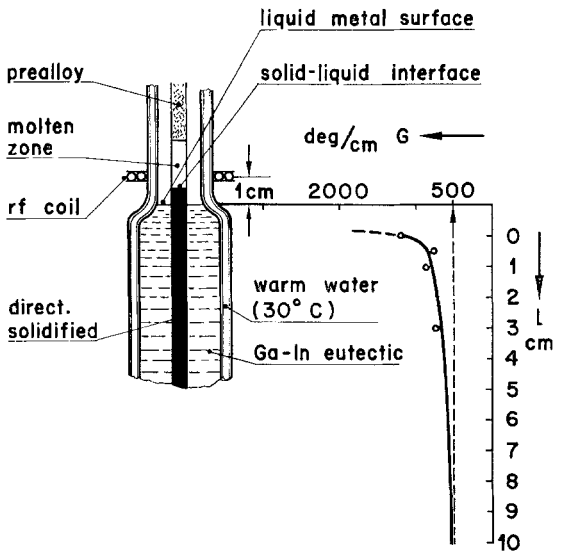

Figure 3 Schematic representation of temperature gradients at the solid-liquid interface as a function of distance between growth front and cooling liquid surface.

A calibration curve showing the temperature gradient dependence of the distance of the solid-liquid interface from the liquid-metal surface is given in fig. 3. The alloy utilised for the measurements was hypereutectic in composition, with a liquidus temperature of 1460°C and a eutectic temperature of 1311°C according to reported DTA data [5]. The gradient was arrived at [9] by measuring the length of primary Cr_7C_3 dendrites growing ahead of the quenched eutectic interface (fig. 4). The quenching was accomplished by dropping the sample containing tube into the Ga–In eutectic coolant (figs. 2b, c and d). The calibration curve is not based on an absolute measurement of the distance between the liquid metal surface of the coolant and the solid-liquid interface of the growing sample, as becomes clear from fig. 3. The curve here is valid for 4 mm diameter samples. 1 mm diameter samples

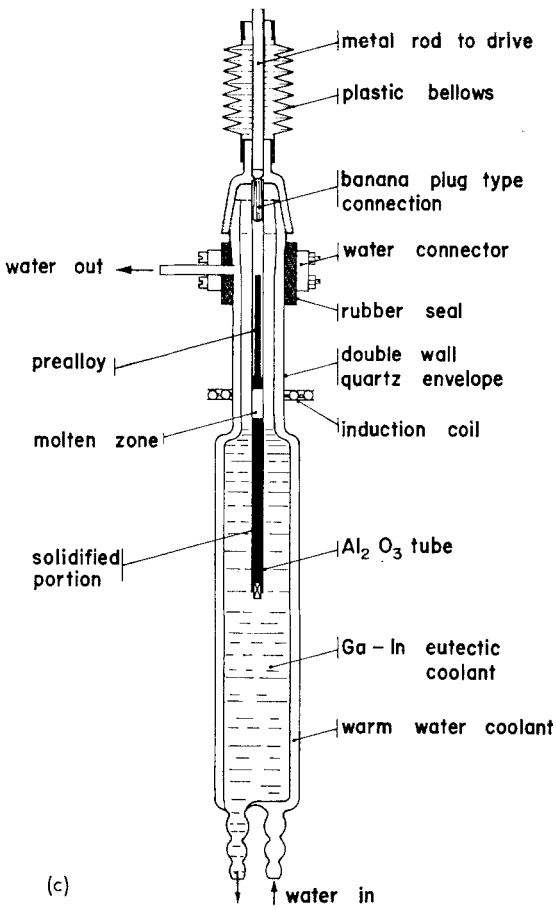

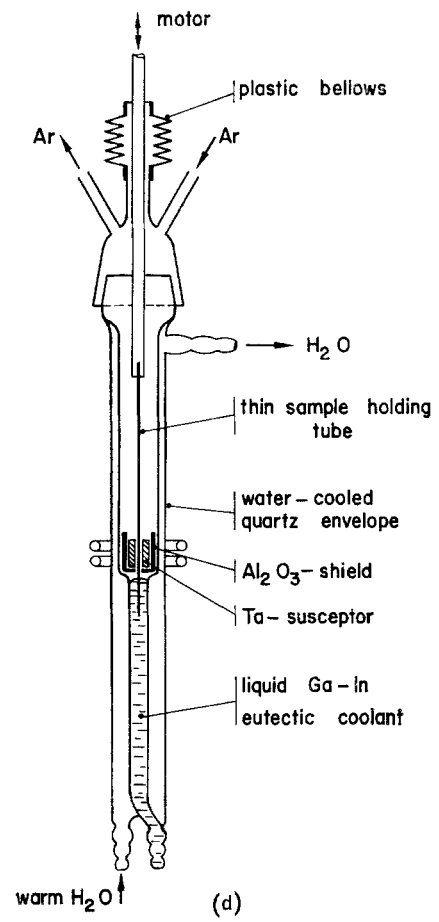

Figure 2 continued

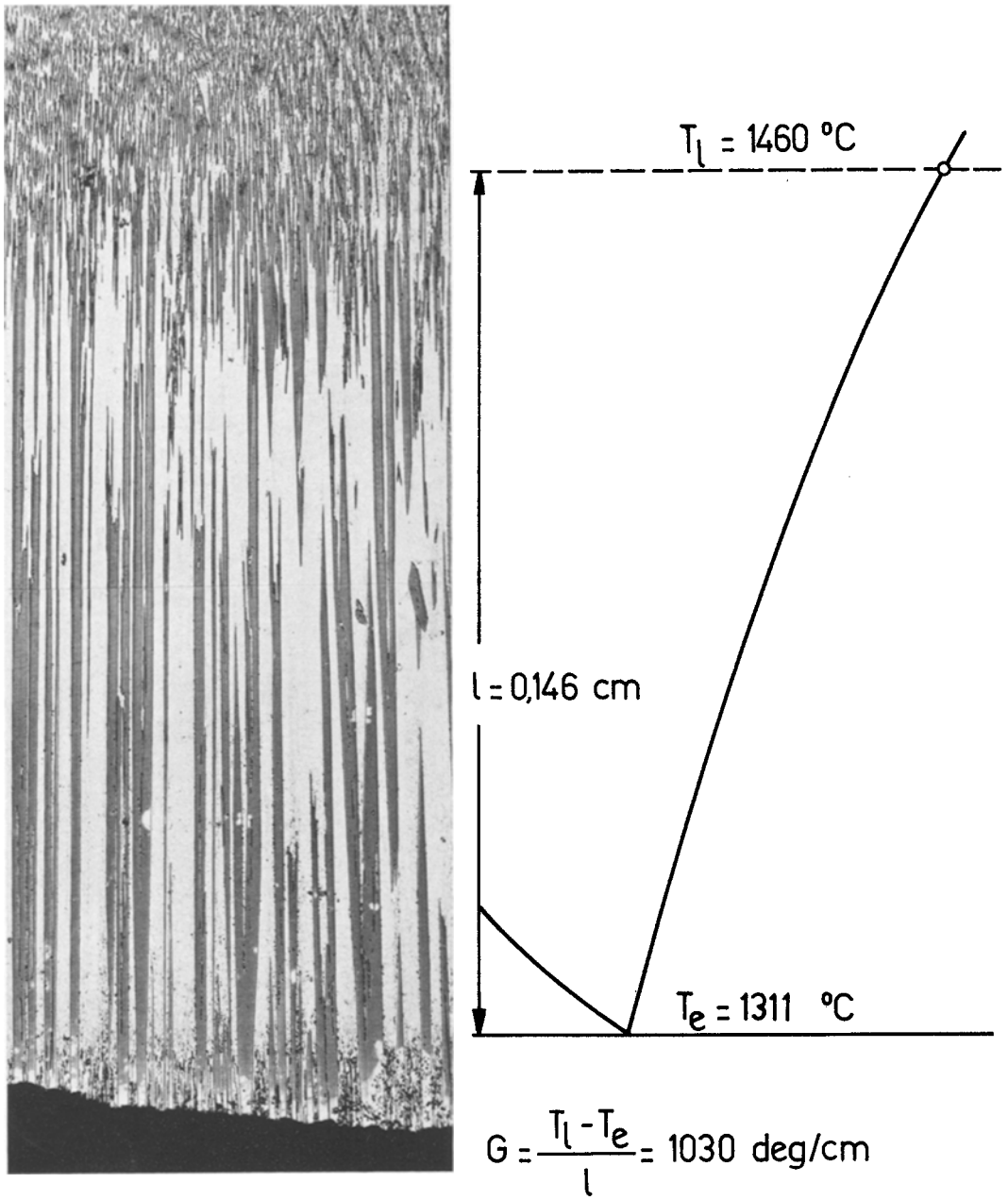

Figure 4 Determination of temperature gradients in the melt ahead of growth front by utilisation of hypereutectic alloys with two solid-liquid interfaces: T (primary carbide needle tips) and T_e (eutectic growth front) [9].

yielded T-gradients up to 3500 deg/cm.

Compositional analysis was carried out by wet chemical methods. Microprobe analysis yielded the phase compositions [6]. Metallographic examination was based mainly on optical microscopy, while some X-ray work and electron microscopy established crystallographic features of the alloys [6].

3. Results

3.1 General Features

The monovariant eutectic Co, Cr (= γ–Co)–

$Cr_{7-x}Co_xC_3$ exhibits a non-variant reaction on a point of the eutectic trough which has a maximum temperature [1, 5, 6]. As seen from fig. 1, the compositions of matrix and carbide are variable over a considerable range and represent two-phase structures of a homogeneous solid solution, γ–Co, and a Berthollide type compound carbide, $Cr_{7-x}Co_xC_3$ (= K_2'). In the phase diagram, the $Cr_{7-x}Co_xC_3$ carbide extends deeply

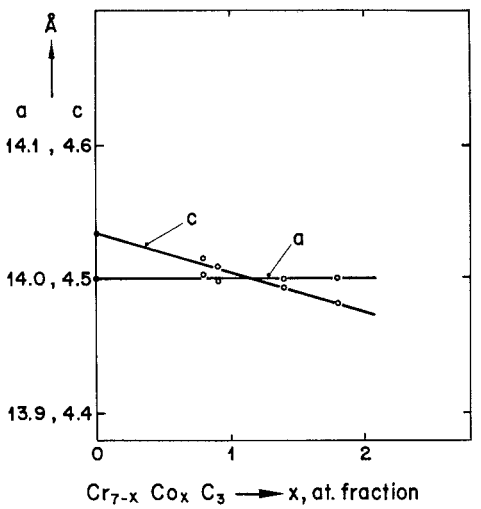

Figure 5 Lattice constants of the carbide $Cr_{7-x}Co_xC_3$ as function of cobalt content.

into ternary space in the form of a sheath. This is supported by determinations of lattice constants of the $Cr_{7-x}Co_xC_3$ carbide [6]. The results in fig. 5 indicate a continuous lattice contraction with increasing Co-content in the direction of the c-axis and no change in the a-direction. From previous work it has also been concluded that the three-phase space (γ–Co + K_2' + L) is very narrow explaining why long ingots with no compositional variation may be directionally solidified anywhere between A_d and D_d (fig. 1). This means, in effect, that an average distribution coefficient [1, 3],

$$\bar{k}_{\alpha,\beta} = \frac{1}{2}\left[\frac{a_1}{a_2}\frac{k_{\alpha 1}}{k_{\alpha 2}} + \frac{b_1}{b_2}\frac{k_{\beta 1}}{k_{\beta 2}}\right] \qquad (1)$$

describing the segregation between α(= γ–Co) and β(= K_2'), must be very nearly equal to 1. Utilising Thompson and Lemkey's criterion [1] for the prediction of well-formed directionally grown structures of monovariant eutectic alloys:

$$G/v \geq \frac{m_t C_0}{D}\left[\frac{1 - \bar{k}_{\alpha,\beta}}{\bar{k}_{\alpha,\beta}}\right], \qquad (2)$$

where m_t = slope of the eutectic trough to either side of the pseudobinary point, D = diffusion coefficient (cm²/sec), C_0 = nominal composition of the alloy, it is, therefore, concluded that $\bar{k}_{\alpha,\beta} \cong 1$ rather than $m_t \cong 0$ is the reason for the large range of obtainable homogeneous directional structures. Previous DTA results [5] have, indeed, shown m_t-values to be not negligible (table II). The liquidus slope of the carbide side is 3.5 times steeper than the one on the matrix side [5] (table II).

TABLE II Melting temperature and eutectic trough slopes of Co, Cr–$Cr_{7-x}Co_xC_3$ alloys.

	Designation*	Thompson and Lemkey [1]	Sahm and Watts [5]
T_e (°C)	Cut 1 (A_d)	1293	1300
	Cut 2 (B_d)	1303	1311
	Cut 3 (C_d)	1290	1306
m_t† (deg/wt fraction)	A_d–B_d	263	262
	B_d–C_d	228	73.5
m_α	On cut B (deg/wt fraction)	—	177
m_β		—	620

*Compare fig. 1.
†Values are arrived at by the approximately correct assumption that the eutectic trough runs along line of constant C-composition, thus only considering changes in Co- or Cr-content.

3.2. Morphology

The compositional homogeneity over a broad range of the eutectic trough is substantiated by the qualitative morphology of the two-phase structures. Fig. 6 shows three micrographs with directionally-grown eutectic and the corresponding quenched interfaces. No obvious differences are detectable.

For the quantitative assessment of fibrous eutectic growth normally the $\bar{R}^2/V$ relationship is utilised, where $\bar{R}$ = 1/2 of the average nearest neighbour interfibre distance and V = growth rate. The $Cr_{7-x}Co_xC_3$ fibres, however, show a much more uneven distribution than is normally found. Therefore, Thompson and Lemkey [1] have proposed to replace $\bar{R}$ by the number of fibres ν, the two quantities being connected by the volume fraction ψ_β of the carbide and the squared average diameter of the fibres $\bar{d}^2$, as follows:

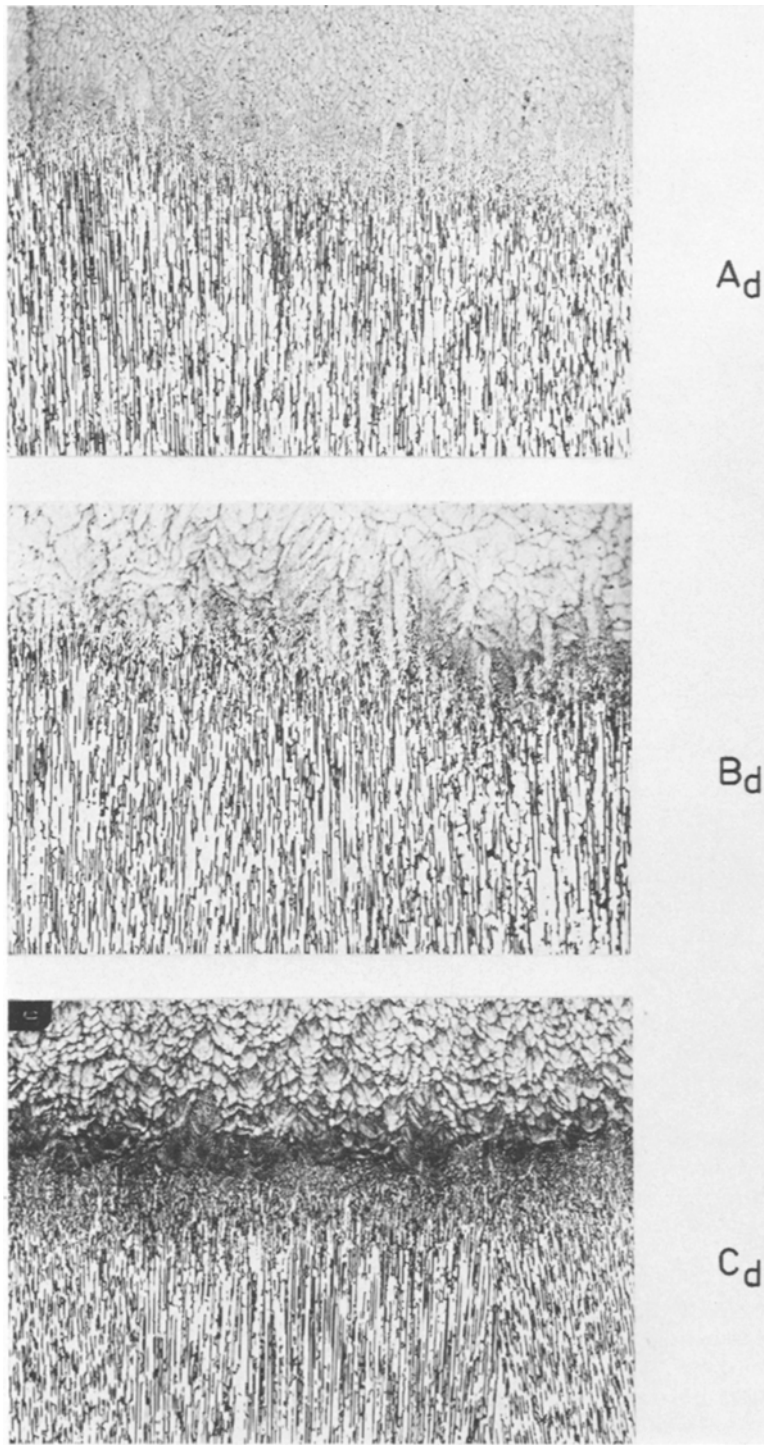

Figure 6 Quenched, rough pseudo-binary eutectic (B_d) and monovariant eutectic (A_d and C_d) interfaces, grown with low temperature gradients.

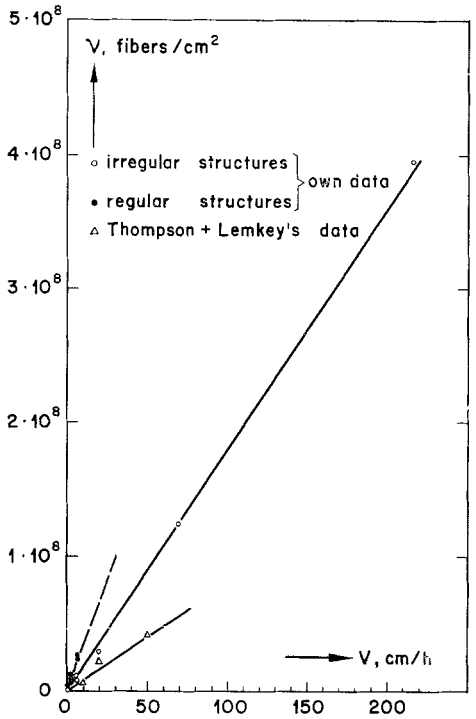

Figure 7 Specific number of fibres ν as function of growth rate v.

$$\psi_\beta = \frac{\pi}{8\sqrt{3}} \frac{\bar{d}^2}{\bar{R}^2} = \nu \frac{\pi \bar{d}^2}{4} \cdot \qquad (3)$$

Thus,

$$\bar{R}^2 v = K \text{ becomes } \frac{v}{2\sqrt{3}\nu} = K \qquad (4)$$

or

$$v/\nu = K', \text{ where } K' = 2\sqrt{3}\, K \,. \qquad (5)$$

In fig. 7 are plotted our data and Thompson and Lemkey's [1] data. The difference is explained on grounds of difficulties in sample taking. In irregular structures (fig. 8) the decision as to which fibres to count as individuals becomes obscured by the many interconnections encountered. The dashed curve in fig. 7 is probably the most reliable one (even though only based on three growth rates) as the employed structures were quite regular (fig. 8) because solidified with high temperature gradients. The constants of equation 4 thus vary between $K = 9 \times 10^{-11}$ and $K = 1.6 \times 10^{-10}$ cm³/sec for our two curves depending on the temperature gradients ($G \cong 3500$ and 500°C/cm, respectively), the first value corresponding to the regular structure.

While the directionality of the two-phase structure was very little affected by the temperature gradient at the solid-liquid interface (well directional fibres, even if in cellular arrangement, were obtained with G-values of $\cong$ 10 deg/cm at $V \cong$ 10 cm/h), very large temperature gradients yielded a more statistically regular fibre distribution as well as a considerably smaller range of fibre diameters (fig. 8). This change in morphological character is paralleled by the type of growth interface encountered which, in turn, is connected with the irregular, "negative dendrite" appearance of the fibres.

3.3. The Solid-Liquid Interface

At larger magnifications attention is focused on the irregularity of the carbide fibres (fig. 6) which may be seen as "negative dendrites", while the matrix appears to have grown by a process generating positive "dendrite shoots". Thus, one may conclude the matrix to be the leading phase at the growth front, with the carbide phase following in the channels left open by the matrix. This first intuitive impression is substantiated by the appearance of quenched solid-liquid interfaces. In most cases (temperature gradients $\simeq$ 500 deg/cm, figs. 6 and 9) the quenched interface showed a diffuse appearance. Further, indirect, evidence supporting the negative dendrite-concept is given by the directional growth of hypereutectic primary carbide crystals such as shown in fig. 4 which, when growing unrestrictedly ahead of the eutectic interface, yield smoothly faceted fibres with no side-shoots. Under more stringent conditions, eutectic carbide fibres may also be smoothed: with high temperature gradients ($G \simeq$ 3500 deg/cm), both a slightly hypo- and a slightly hyper-eutectic composition of cut 1 (compositions $A_{e/d}$ and A_e, fig. 1) displayed nearly "classical interfaces" (referring to the model discussed by Jackson and Hunt [7]), as seen in fig. 10. High temperature gradients, besides leading to a more regular distribution and a smaller range of fibre diameters, also yielded smoother fibres (fig. 11b).

In conclusion, the mode of growth may be characterised by the sketch in fig. 12, which illustrates the matrix phase growing ahead in the form of dendrite tips. The carbide follows in the channels left open by these dendrites arranged in a most closely packed manner in the sketch. This arrangement appears to be quite realistic; in fig. 13 an array of nearly close packed circles has been sketched into a micrograph of a typical

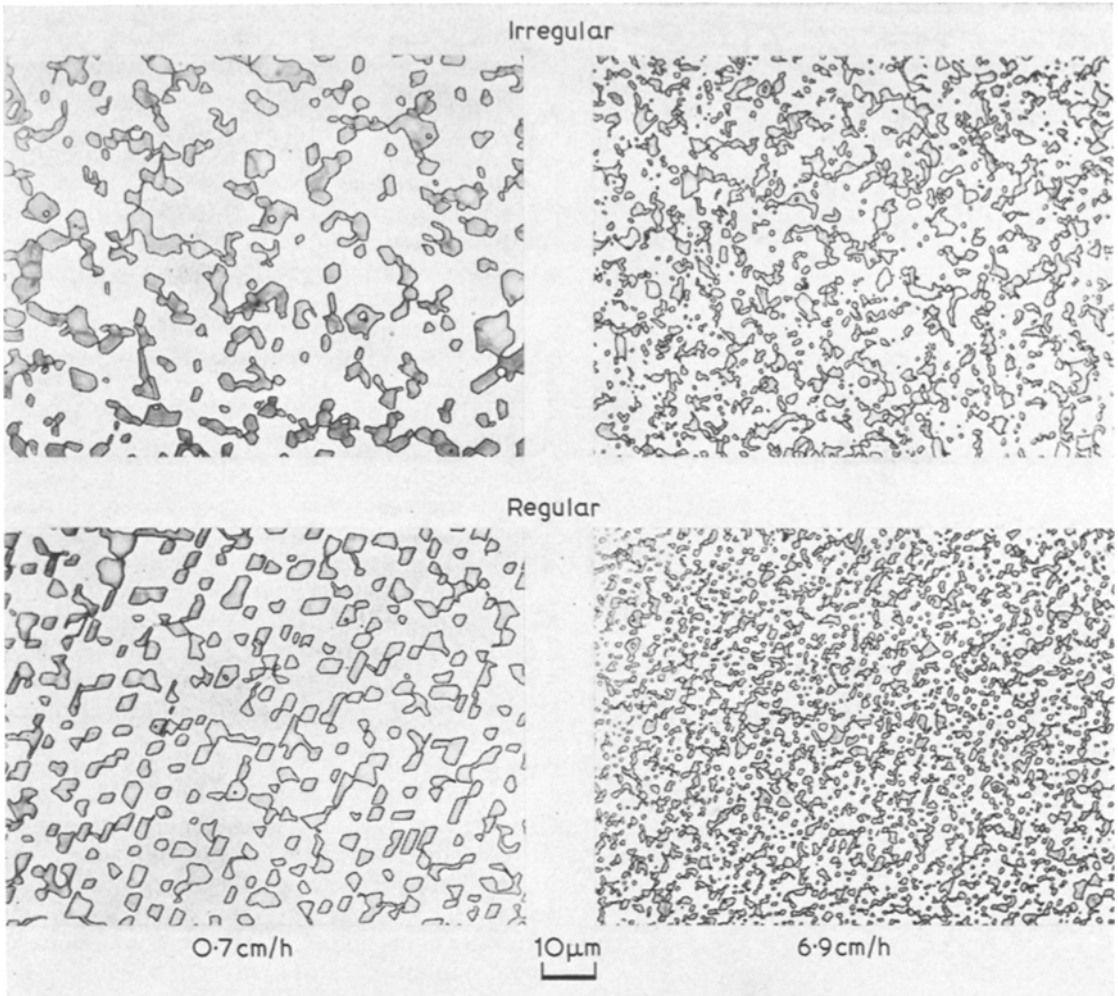

Figure 8 Regular and irregular two-phase structures of the Co, $Cr–Cr_{7-x}Co_xC_3$ eutectic.

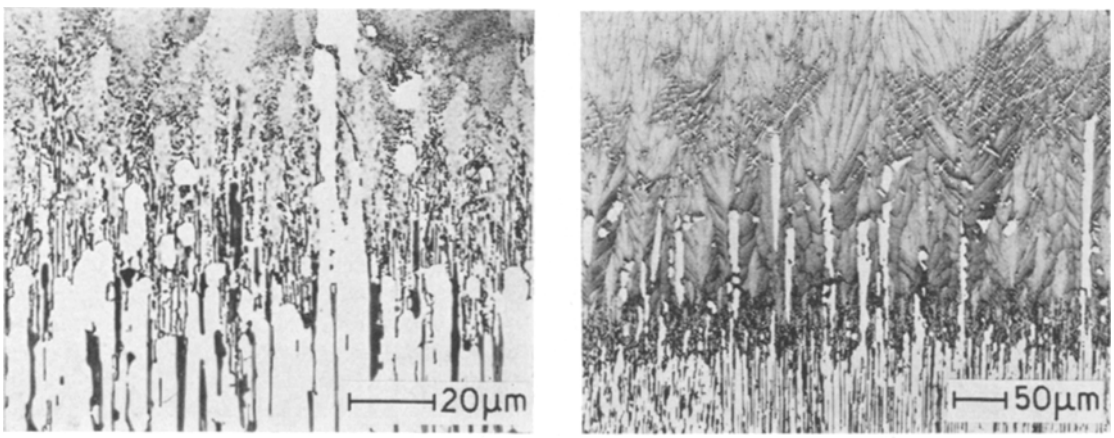

Figure 9 Quenched interfaces showing leading dendrite-like matrix phase.

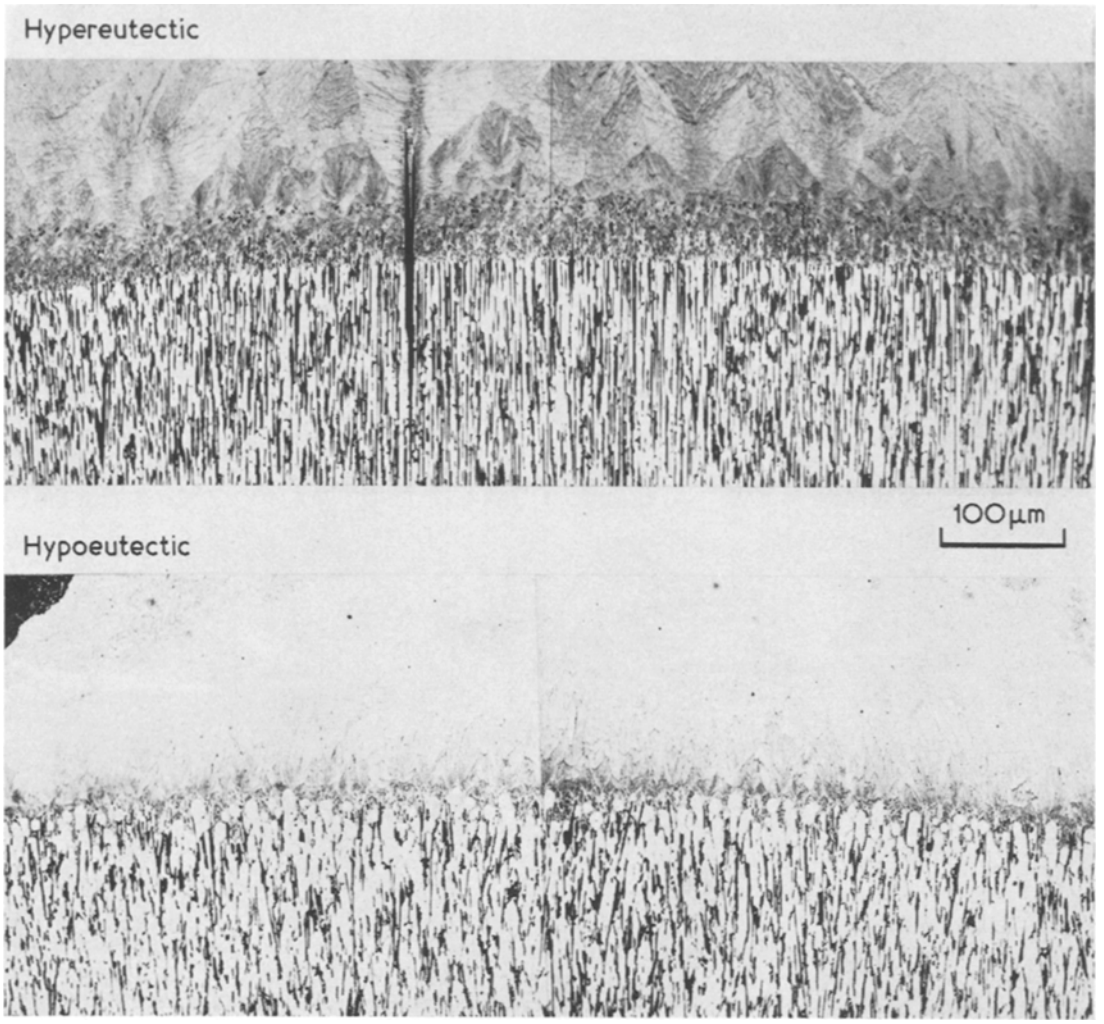

Figure 10 Smooth, quenched hypereutectic (= carbide rich) and hypoeutectic (= matrix rich) interfaces, grown with large temperature gradients.

structure, solidified with $G \simeq 500$ deg/cm, yielding very nearly the stylised picture of fig. 12. For G-values below 500 deg/cm one may approximate the morphology by considering a skeleton of carbide encompassing large fibres of matrix whose tips grow dendritic-like into the melt approximating a closely packed array of cylinders (figs. 12 and 13). The remaining voids between the dendrite tips are then filled by carbide. Fortunately, its volume fraction of 30% approximates the theoretical void space of 26% present in such an array.

4. Discussion

In the light of results with other faceted-nonfaceted eutectic systems, for example Al–Si or Fe–C, the strongly coupled growth found in Co, $Cr–Cr_{7-x}Co_xC_3$ alloys is unexpected.

Referring to the model presented in figs. 12 and 13 one may liken the growth mode of the matrix to dendrite peaks growing ahead of the solid-liquid interface of the carbide which forms a network of interconnected, hexagonally faceted, fibres. The strong coupling between matrix and carbide, i.e. the high directionality of growth, is considered to be due to the thermodynamic crystallographic, and kinetic properties of the pseudobinary system, as follows:

a. Advantageous volume fractions of the phases: the quasi-hexagonally close-packed pat-

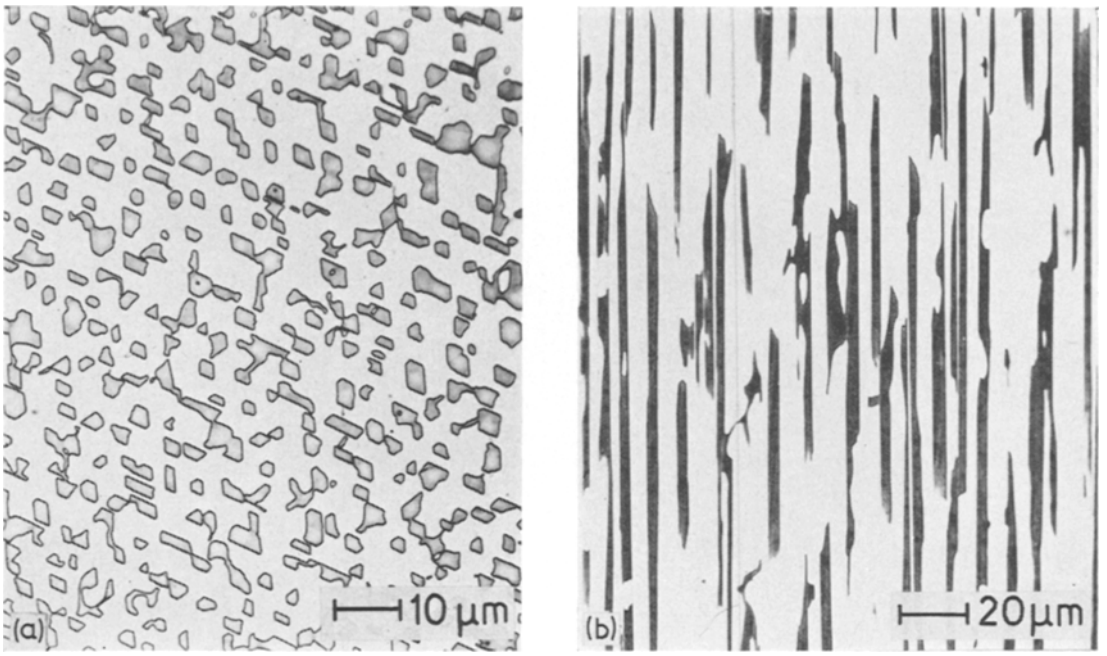

Figure 11 Smooth fibres of eutectic structure obtained with large temperature gradients.

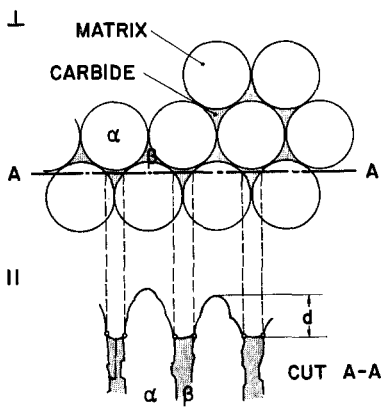

Figure 12 Stylised arrangement of matrix-carbide phases in Co, $Cr–Cr_{7-x}Co_xC_3$ eutectic. Concentration and temperature profiles indicate assumed behaviour.

tern of the matrix-dendrites (about 70% closely approaching the theoretical 74%) allows for relatively short mean lateral diffusion distances between the two crystallising phases. This may help explain the fibrous nature of the eutectic despite its relatively high volume fraction of carbide (which would normally result in a lamellar morphology).

b. High growth rate anisotropy of the carbide: Looking at the atom packing [8] (fig. 14) suggests a possible reason for the *c*-axis to grow parallel to the growth direction. The alternating deposition of 9, 12, 9, 12 Cr- and Co-atoms (with intermittent depositions of C-atoms which are omitted in fig. 14) guarantees a rather smoothly continuous deposition rate of atoms. In agreement with Thompson and Lemkey's findings [1] we also observed the carbide to grow in the [0001] and the matrix in the [211] direction independent of the position on the eutectic trough (fig. 1). The electron diffraction patterns showed an angle of about 20° (tan 18.4° = 1/3) to occur reproducibly between the carbide and matrix lattices, indicating that the carbide-matrix interface energy must play a certain role and probably is minimised by this configuration. The high growth rate anisotropy of the carbide induces its fibres to grow obstinately in one crystallographic direction, thus providing a rigid carbide network which forces the matrix dendrites to maintain unidirectionality on account of a sufficiently small lead distance (5 to 10 μm). Normally, dendritic growth would tend to seriously upset directionality of a composite structure. An

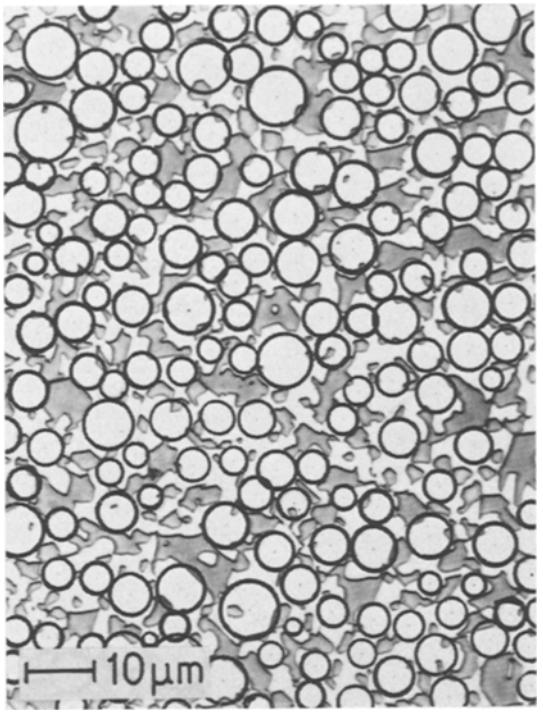

Figure 13 Array of circles fitted around free matrix areas.

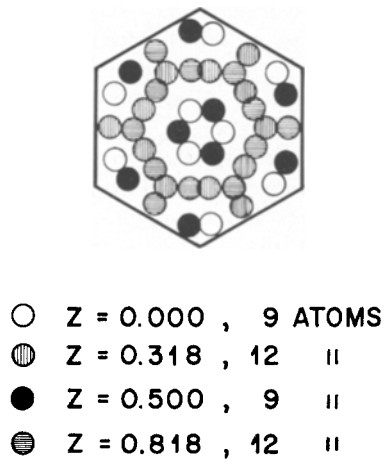

Figure 14 Atom packing of $Cr_{7-x}Co_xC_3$ carbide only, showing Co- and Cr-atoms which are indistinguishable.

example for this tendency may be appreciated upon examination of the hypoeutectic, i.e. Co-rich structure in fig. 10. Here the larger lead of the γ-Co dendrites leaves room for stronger deviation from directionality.

c. Larger undercooling of the carbide/melt interface owing to growth-inhibition (kinetic undercooling) and the steeper liquidus slope of the carbide (volume diffusional undercooling): The kinetic undercooling $\Delta T_{k,c}$ corresponds to a supersaturation of $\Delta c_c = |c_e - c'_e|$ – see fig. 15a. This carbide undercooling displaces the eutectic point from the equilibrium position characterised by T_e and c_e to T_e' and c_e' (fig. 15). The actual composition, which is, in effect c_e, would then be in the hypoeutectic region of the new "kinetic phase diagram" and thus provide an explanation for the dendritic type growth of the matrix (fig. 12). The temperature profile ahead of the crystallisation front has likewise been sketched in fig. 15. The "relative kinetic undercooling" of the carbide, $\Delta T'_{k,c}$ (fig. 15a), requires a concave interface carbide-melt (compare figs. 9 and 12), i.e. a "curvature overheating" – as against the curvature undercooling of the convex matrix dendrite – melt interface. Since the undercooling or overheating of a phase due to its interface curvature, generally, is inversely proportional to its specific heat of fusion, which is higher in the carbide, this effect will not be able to compensate completely both the large kinetic and volume diffusional undercoolings of the carbide. The effect of the resulting anisothermicity of the interface as it is sketched in fig. 15b is probably further attenuated by the larger production of heat of solidification by the carbide which, in turn, avoids constitutional supercooling in the liquid void space between matrix dendrites by shifting the melt temperature towards equilibrium liquidus temperature. These counterbalancing features give rise to a steady propagation mode of an essentially non-isothermal solidification interface.

With respect to the morphology, the growth process still stays volume-diffusion-limited. This is concluded from the observation that the $R^2v = K$-relationship holds, even though the constant K appears to have become a function of the temperature gradient

$$K = K(G) \ . \qquad (6)$$

Examination of the expression (4) derived [7, 10] for K does not suggest an obvious relationship. It rather must be understood as a matter of sample taking, i.e. the number of fibres which increases with higher G by evening out the interface shape, thus approaching the idealised assumption [7] of a flat interface.

With higher G-values the bridging between the

TABLE III Examples of two-phase alloys of the type MeCr–$Cr_{7-x}Me_xC_3$ (Me = Mn, Fe, Co, Ni).

Sample number	Matrix wt % Mn	Fe	Co	Ni	Cr	Carbide wt % Mn	Fe	Co	Ni	Cr	C	Formula (approximated)
213	—	84.5	—	—	15.5	—	36	—	—	56	8	$Cr_{4.5}$ $Fe_{2.5}$ C_3
D_f	—	—	84	—	16	—	—	22	—	69	9	$Cr_{5.4}$ $Co_{1.6}$ C_3
	—	—	—	80	20	—	—	—	6	85	9	$Cr_{6.6}$ $Ni_{0.4}$ C_3
781	5.5	—	65	—	29.5	2.2	—	10	—	79	9	$Cr_{6.1}$ $Co_{0.7}$ $Mn_{0.2}$ C_3
788	—	7	65	—	28	—	2	10	—	79	9	$Cr_{6.15}$ $Co_{0.7}$ $Fe_{0.15}$ C_3
782	—	—	63.5	7	29.5	—	—	10	0.6	80.5	9	$Cr_{6.25}$ $Co_{0.7}$ $Ni_{0.05}$ C_3
786	4.5	5	58	4.5	28	2	1.25	9	0.25	78.5	9	$Cr_{6.2}$ $Co_{0.7}$ $Ni_{0.05}$ C_3

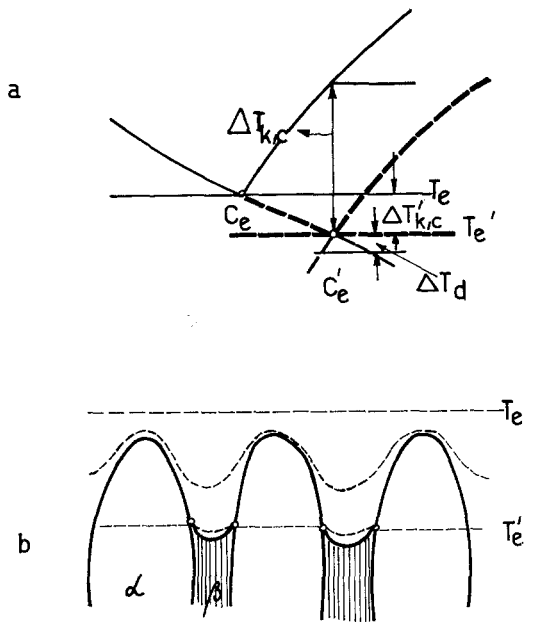

Figure 15 Displacement of eutectic point due to kinetic undercooling of carbide (a) and resulting temperature profile at interface (*b*).

carbide fibres is also eliminated and the interface becomes more isothermal (fig. 8). The carbide pattern (fig. 13) has its weakest links at the void triangle corners such that the transition from this strongly-interconnected morphology (fig. 13) to the regular, discrete, morphology (fig. 11) may be assumed to start by separation at these intersections of {100} facets.

5. Outlook

It is obvious that alloys of the kind described above open up an alloyer's "eldorado" as both matrix and carbide may be added to or subtracted from by substituting elements. For example, alloys of the type compiled in table III have been synthesised, indicating that Mn, Fe, Co, Ni can be substituted with decreasing readiness in the order enumerated here. The resulting morphologies [11] are quite comparable to each other, showing the same type of irregular dendrite-like but well-oriented structure with equally diffuse interfaces but strongly coupled growth behaviour as found in the Co–Cr–C alloys described above (fig. 15).

Alloys of the type discussed here may permit one to tailor-make alloys with desired properties on a hitherto unforeseen scale. Several examples have already been presented [12]. For example, the juxtaposition of the three ternary diagrams [13-15] in fig. 16 suggests that, because similar phase fields exist in all cases, shifts of phase-separating lines occurring upon cross-alloying should be reasonably well predictable. Their controlled solidification with little or no macro-segregation over large volumes may be more readily achieved than in simple (two-component) two-phase alloys because the more complex ternary (or polynary) phases normally are more complex crystallographically resulting in phenomena such as those described in this paper [16, 17]. What remains to be done is the generation of thermodynamic data on ternary and multi-component systems to find suitable monovariant reactions.

6. Conclusions

From investigations into the solidification behaviour conducted with Co, Cr–$Cr_{7-x}Co_xC_3$ alloys the following conclusions have been reached.

a. Monovariant eutectic two-phase structures of the type Co, Cr–$Cr_{7-x}Co_xC_3$ exhibit very

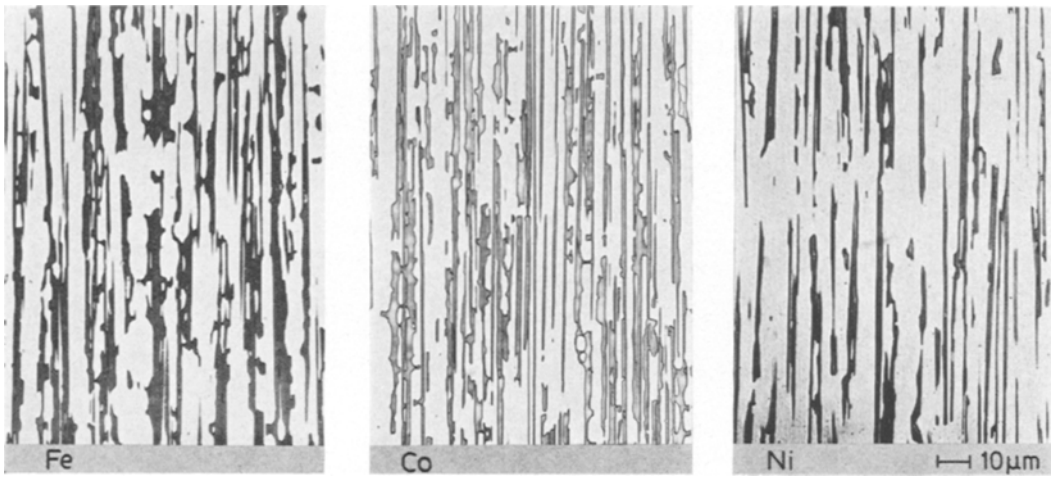

Figure 16 Similarity of monovariant eutectic structures of the type Me, Cr–$Cr_{7-x}Me_xC_3$ with Me–Fe, Co, Ni.

strongly coupled growth over a large regime of conditions.

b. For all growth rates and temperature gradients below approximately 500 deg/cm the structure is determined by a solid-liquid interface characterised by a close packed pattern of leading matrix dendrite tips with the carbide phase growing behind in the voids left open by the dendrite tips and representing a highly interconnected network of needle-like morphologies.

c. The carbide grows with a highly anisotropic growth rate with the highest value in the [0001] direction.

d. For temperature gradients of approximately 3500 deg/cm the lead distance of the matrix dendrite tips decreases, resulting in a more regularly random distribution of and fewer interconnections between carbide fibres as well as in a smaller range of fibre diameters. All in all, this means a more regular structure.

e. The eutectic grows with an appreciable kinetic undercooling and a slightly non-isothermal interface.

Acknowledgements

For carrying out the experimental work we wish to thank Mrs R. Sebalj (directional solidification), Mrs B. Höhn (metallography), and Dr W.

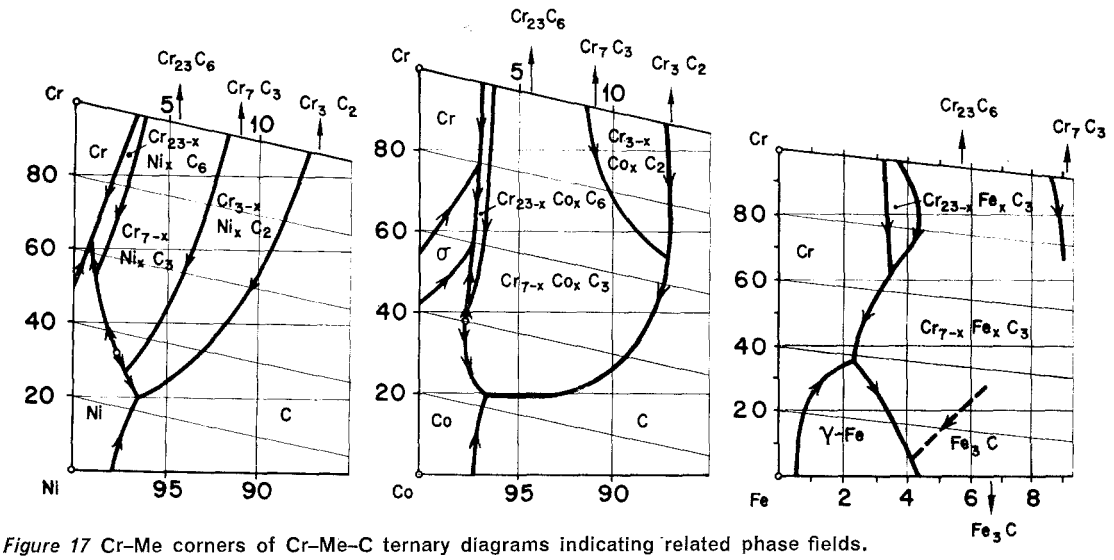

Figure 17 Cr–Me corners of Cr–Me–C ternary diagrams indicating related phase fields.

Hugi (microprobe analysis). For fruitful discussions we would like to thank Drs D. J. Rowcliffe and F. D. Lemkey.

References

1. F. D. LEMKEY and E. R. THOMPSON, *Metall. Trans.* **1** (1970) 2799.
2. H. E. BATES, F. WALD, and M. WEINSTEIN, *J. Mater. Sci.* **4** (1969) 25.
3. P. R. SAHM and M. LORENZ, to be published in *Werkstofftechnik*.
4. J. D. HUNT and K. A. JACKSON, *Trans. AIME* **236** (1966) 843.
5. P. R. SAHM and D. J. WATTS, *Metall. Trans.* **2** (1971) 1260.
6. P. R. SAHM, M. LORENZ, W. HUGI, and V. FRÜHAUF, *Metall. Trans.* to be published.
7. K. A. JACKSON and J. D. HUNT, *Trans. AIME* **236** (1966) 1129.
8. S. NAGAKURA and S. OKETANI, *Trans. Iron Steel Inst. Japan* **8** (1968) 265.
9. R. M. SHARP and A. HELLAWELL, *J. Cryst. Growth*, **6** (1971) 253.
10. P. R. SAHM *Schweiz. Archiv*, **36** (1970) 165.
11. J. VAN DER BOOMGAARD, personal communication and paper presented at International Conf. on Crystal Growth, Marseille 1971 (paper No. B7-5).
12. J. A. BATT, F. DOUGLAS, and E. R. THOMPSON, 139th Meeting Electrochemical Society, Washington 1971 (Abstract No. 150).
13. W. KÖSTER and F. SPERNER, *Arch. Eisenhow.* **26** (1955) 555.
14. W. KÖSTER and S. KABERMANN, *ibid* **26** (1955) 627.
15. R. S. JACKSON, *J. Iron Steel Inst.* 208 (1970) 163.
16. H. E. CLINE and J. L. WALTER, *Metallurg. Trans.* **1** (1970) 2907.
17. P. R. SAHM, paper presented at Hauptversammlung der Gesellschaft Deutscher Chemiker, Karlsruhe 1971 (to be published in *Giessereiforschung*).

Received 1 November and accepted 10 December 1971